analytical chemistry

pubs.acs.org/ac

Article

Explaining the Decay of Nucleic Acid-Based Sensors under Continuous Voltammetric Interrogation

Vincent Clark,[#] Miguel Aller Pellitero,[#] and Netzahualcóyotl Arroyo-Currás*

Cite This: *Anal. Chem.* 2023, 95, 4974−4983

Read Online

ACCESS | Metrics & More | Article Recommendations | Supporting Information

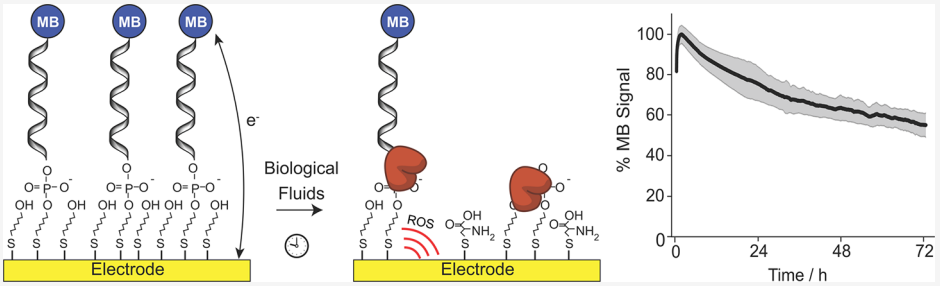

ABSTRACT: Nucleic acid-based electrochemical sensors (NBEs) can support continuous and highly selective molecular monitoring in biological fluids, both in vitro and in vivo, via affinity-based interactions. Such interactions afford a sensing versatility that is not supported by strategies that depend on target-specific reactivity. Thus, NBEs have significantly expanded the scope of molecules that can be monitored continuously in biological systems. However, the technology is limited by the lability of the thiol-based monolayers employed for sensor fabrication. Seeking to understand the main drivers of monolayer degradation, we studied four possible mechanisms of NBE decay: (i) passive desorption of monolayer elements in undisturbed sensors, (ii) voltage-induced desorption under continuous voltammetric interrogation, (iii) competitive displacement by thiolated molecules naturally present in biofluids like serum, and (iv) protein binding. Our results indicate that voltage-induced desorption of monolayer elements is the main mechanism by which NBEs decay in phosphate-buffered saline. This degradation can be overcome by using a voltage window contained between −0.2 and 0.2 V vs Ag|AgCl, reported for the first time in this work, where electrochemical oxygen reduction and surface gold oxidation cannot occur. This result underscores the need for chemically stable redox reporters with more positive reduction potentials than the benchmark methylene blue and the ability to cycle thousands of times between redox states to support continuous sensing for long periods. Additionally, in biofluids, the rate of sensor decay is further accelerated by the presence of thiolated small molecules like cysteine and glutathione, which can competitively displace monolayer elements even in the absence of voltage-induced damage. We hope that this work will serve as a framework to inspire future development of novel sensor interfaces aiming to eliminate the mechanisms of signal decay in NBEs.

INTRODUCTION

Nucleic acid-based electrochemical sensors (NBEs) are modular analytical platforms that can enable continuous molecular sensing regardless of target reactivity.[1−3] This ability originates from the use of biomolecular recognition elements that allow affinity interactions to probe target concentrations (e.g., aptamers and[4,5] antibodies[6]). In more detail, NBEs typically consist of mixed monolayers containing blocking alkylthiols and a redox reporter, thiol-functionalized oligonucleotides self-assembled on gold electrodes (Figure 1A).[7] The possibility to design nucleic acids so they undergo target-binding induced conformational changes[8] allows continuous molecular monitoring via serial electrochemical interrogation of the reporter.[9] This is possible because in NBEs, the electron transfer rate is an exponential function of the distance between the redox reporter and the electrode surface.[10,11] Thus, reversible target binding that changes the three-dimensional positioning of the nucleic acid-bound reporter relative to the electrode surface affects NBE signaling to an extent proportional to the target concentration.[12] For example, previous studies have demonstrated continuous molecular monitoring of proteins in biofluids using a voltage-actuated, DNA-based molecular pendulum.[6] Likewise, single-stranded nucleic acid aptamers have been used for continuous molecular monitoring of small-molecule therapeutics in vivo.[5] Unfortunately, the thiol-based monolayers used for the fabrication of NBEs are not stable in biological fluids, a problem that limits the operational life of such sensors to periods of hours.[13,14] This

Received: November 18, 2022
Accepted: February 23, 2023
Published: March 7, 2023

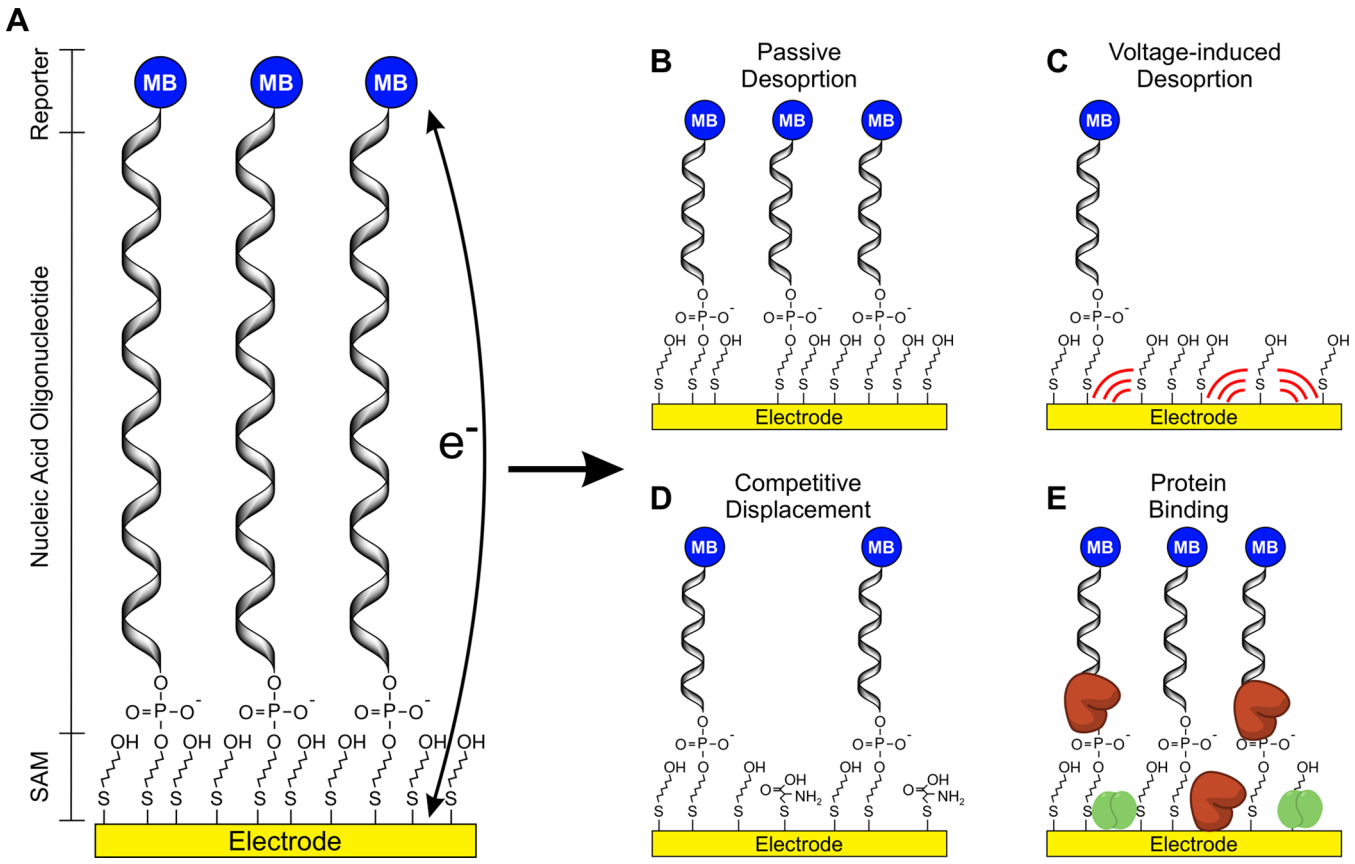

Figure 1. Nucleic acid-based sensors (NBEs). (A) Anatomy of NBEs can be broadly broken down into three main elements: a self-assembled monolayer of short-chain alkylthiols, alkylthiol-modified nucleic acid oligos, and redox reporters covalently bound to the nucleic acids, here methylene blue (MB). This interface can decay via: (B) passive desorption of monolayer elements from the sensor surface in the absence of a voltage bias, (C) voltage-induced desorption, (D) competitive displacement by thiolated molecules naturally occurring in biological fluids, and (E) non-specific protein binding.

lifetime is not sufficiently long to enable the successful translation of NBEs to wearable or implantable biomedical platforms requiring in vivo exposure for several days or weeks.[15,16] Thus, there remains an unmet need to further understand NBE degradation pathways and to develop novel monolayer chemistries that overcome the lability of thiol-gold bonds to enable multiday and multiweek sensing in vivo.

The ability to develop novel strategies to reduce or eliminate monolayer loss in NBEs strongly depends on our understanding of DNA monolayer decay mechanisms in buffered solutions as well as in biofluids like serum. To date, our group and others have experimentally identified key sources of NBE monolayer loss under continuous electrochemical interrogation. Briefly, Shaver et al. showed that the hydrophilicity of benchmark 6-mercapto-1-hexanol (MCH) blocking monolayers significantly increases their rate of desorption from the sensor surface in aqueous media relative to hydrophobic monolayers of 1-hexanethiol, causing progressive sensor signal loss.[14] The same authors demonstrated that nuclease-driven hydrolysis of DNA aptamers is not a major driving force of signal decay in biofluids over periods of 4 h.[13] In contrast, Pellitero et al. demonstrated that the electrochemical interrogation of the sensors itself can strongly accelerate monolayer loss.[17] This observation was also reported by Leung et al.,[18] who additionally demonstrated that the voltage range used for sensor interrogation plays an important role in NBE stability. Furthermore, Li et al. showed that non-specific protein binding to sensor surfaces can restrict the conformational changes needed for NBE sensing, affecting sensor signaling output.[19] Overall, these works have highlighted that sensor degradation is co-dependent on electrochemical interrogation parameters and biochemical environment.

Seeking to further expand our understanding of NBE decay, this study shows the effect that voltage window, interrogation frequency, and square wave frequency have on sensor signaling lifetimes in buffered solutions. Our results indicate that the applied voltage window during sensor interrogation is the most important driving force for sensor signal decay. Confining the interrogation window to a voltage range between −0.2 and 0.2 V vs Ag/AgCl completely eliminates signal decay within 24 h of repetitive, high-frequency sensor interrogation. This result in turn highlights the need for alternative redox reporters with more positive reduction potentials than the benchmark methylene blue ($E^{0\prime} \sim -0.24$ V). Additionally, we developed serum mimetics to study competitive displacement, a mechanism through which thiolated molecules naturally occurring in biofluids like serum can displace NBE monolayer elements, further driving rapid signal loss. We demonstrate that the combination of voltage-induced monolayer desorption and competitive displacement, which occur simultaneously in biofluids in vitro and in vivo, are the main drivers of short-term NBE signal decay. This work provides a reference framework to guide future efforts to optimize sensor interrogation and mitigate the mechanisms of NBE signal

https://doi.org/10.1021/acs.analchem.2c05158
Anal. Chem. 2023, 95, 4974−4983

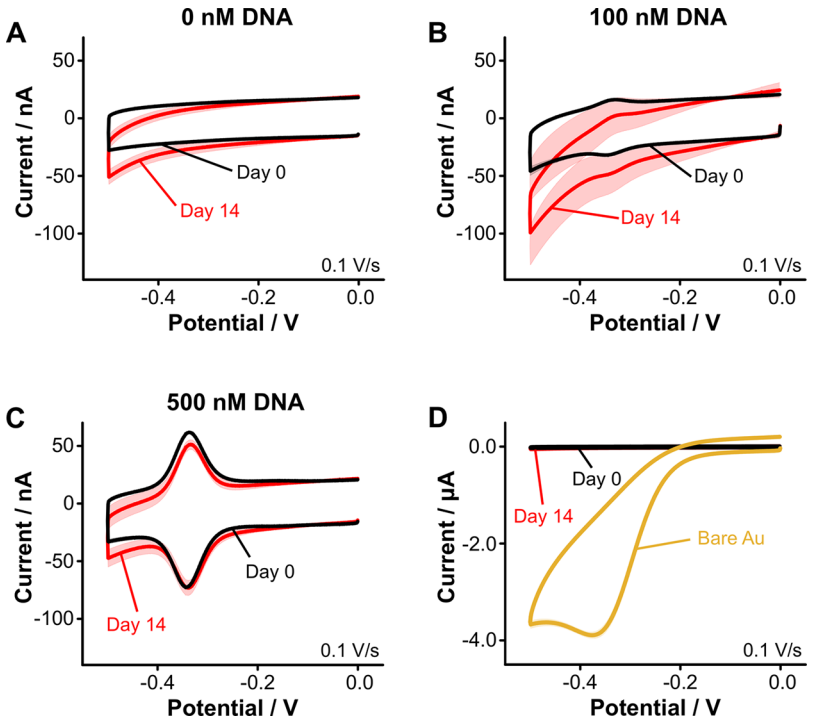

Figure 2. NBEs remain stable in buffered saline when not subjected to frequent voltage scanning. Cyclic voltammograms measured on NBEs functionalized with a blocking monolayer of mercaptohexanol (MCH) and DNA at packing densities of (A) Γ_{0nM} = 0 pmol/cm^2, (B) Γ_{100nM} = 0.53 ± 0.07 pmol/cm^2, and (C) Γ_{500nM} = 3.94 ± 0.25 pmol/cm^2 display a 50% increase in oxygen reduction currents at −0.5 V vs AglAgCl. The voltage scanning rate was 0.1 V/s. However, the sensors showed no significant change in capacitive currents at −0.1 V. The top labels indicate molar DNA concentrations used during electrode functionalization. (D) Relative to the large oxygen reduction and capacitive currents seen for bare, unfunctionalized gold electrodes (yellow trace), the changes in current observed in NBEs (black and red traces) over the 14-day period are negligible, an indication that the blocking monolayer remains mostly intact over this period. In all panels, solid lines and shaded areas represent the average and standard deviation of n = 6 sensors.

loss toward translation of these platforms to multiday and multiweek in vivo sensing.

METHODS

DNA Preparation. To prepare ssDNA solutions, we incubated 1 μL ssDNA solution (100 μM in phosphate-buffered saline [PBS]) with 2 μL of a TCEP solution (5 mM in water) for 1 h to reduce disulfide bonds. Afterward, we diluted the DNA in PBS to a final concentration of 500 nM, as determined via absorbance measurements using an Implen Nanophotometer NP80.

Electrode Preparation. We polished gold electrodes for ∼4 min using first a silicon carbide paper and then a cloth pad with (1 μm diameter) alumina slurry. After polishing, the electrodes were rinsed with deionized water, sonicated (in the water) for 30 s to remove any remaining alumina debris, and activated via cyclic voltammetry in 0.5 M NaOH and 0.5 M H_2SO_4 following previously reported protocols.[20,21] Electrodes were then immediately placed into 500 nM solutions of DNA for 90 min. Following DNA incubation, we placed the electrodes into a freshly made 1 mM solution of MCH for 12 h. After a final rinsing with deionized water, the electrodes were ready for use.

Electrochemical Measurements. CH Instruments Electrochemical Analyzer (CHI 1040C, Austin, TX) multichannel potentiostats and associated software were used for all electrochemical measurements. A three-electrode cell configuration consisting of a gold working electrode, a coiled platinum wire counter electrode, and an Ag/AgCl reference electrode was used. All stability square wave voltammetry measurements used a voltage window from −0.1 to −0.5 V, an amplitude of 50 mV, a step of 1 mV, and a frequency of 250 Hz after a quiet time of 2 s. For the continuous voltammetric interrogation, we kept the electrodes at 25° C using a water bath circulator. All cyclic voltammetry measurements used a voltage window from 0 to −0.5 V and a scanning rate of 0.1, 1, and 5 V/s after a quiet time of 2 s.

Data Analysis. To process the files generated during the continuous voltametric interrogation, we used a Python-based custom script previously reported by our group (SACMES).[22] SACMES allows the fast extraction of capacitive and faradaic currents from voltammograms, thus enabling batch analysis of the thousands of files generated during stability measurements.

RESULTS AND DISCUSSION

Our strategy to study NBE stability is based on serially interrogating sensors via cyclic and square wave voltammetry in media of varying compositions to independently evaluate mechanisms of signal degradation (Figure 1B−E).[23] We use cyclic voltammetry to track changes in the oxygen reduction and capacitive currents resulting from the loss and/or reorganization of blocking monolayer elements on the electrode surface.[24] As a complementary technique, we use square wave voltammetry to monitor with high sensitivity changes in electron transfer originating from the loss of reporter-modified oligos from the electrode surface.[14] As model systems, this work uses NBEs functionalized with ssDNA oligos; however, the decay mechanisms revealed here

https://doi.org/10.1021/acs.analchem.2c05158
Anal. Chem. 2023, 95, 4974−4983

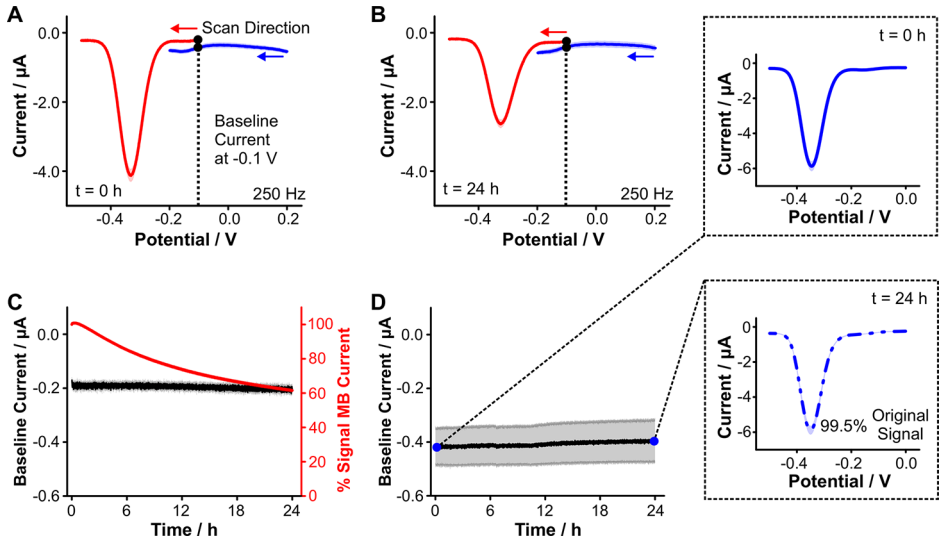

Figure 3. NBE stability strongly depends on the voltage window. We interrogated two batches of identical NBEs every 7 s for 24 h via square wave voltammetry. Batch 1 (red traces) was interrogated across the voltage window from −0.1 to −0.5 V. Batch 2 (blue traces) was interrogated from 0.2 to −0.2 V. The resulting voltammograms at t = 0 h (A) and t = 24 h (B) reveal a 40% loss in voltammetric peak currents for Batch 1. (C) However, no changes in capacitive currents (black traces) for Batch 1 are observed over the measurement period, an indication that the blocking monolayers are intact. (D) Similarly, the capacitive currents from Batch 2 remain flat over the 24 h period. However, in contrast to Batch 1, voltammograms from Batch 2 measured over the methylene blue window once at t = 0 h and once at t = 24 h (after 12,000 scans) showed a 99% retention of methylene blue's voltammetric currents (dashed panels). Solid and dashed lines and their respective shaded areas represent the average and standard deviation of n = 6 electrodes.

should also affect, to varying extents, NBEs based on duplex DNA[6] or other oligo types.[13,23]

Alkylthiol-Modified DNA Monolayers Are Stable for Weeks if Left Undisturbed. We first investigated the stability of freshly fabricated NBEs when stored in phosphate-buffered saline under minimal voltage perturbations for 2 weeks. Because NBE monolayers are self-assembled from bulk alkylthiol and alkylthiol-modified oligo solutions, we hypothesized that storing the sensors in buffered saline in the absence of monolayer elements in the bulk solution would cause a slow but measurable passive desorption process (Figure 1B).[25] To evaluate this effect, we fabricated three batches of six sensors each using different aptamer deposition concentrations: 0 nM (Γ_{0nM} = 0 pmol/cm^2), 100 nM (Γ_{100nM} = 0.5 ± 0.1 pmol/cm^2), and 500 nM (Γ_{500nM} = 3.9 ± 0.3 pmol/cm^2). We then measured the voltammetric response of these sensors at t = 0 h and then every 72 h (i.e., every 3 days) for a period of 14 days. Following each measurement, we placed the sensors in fresh buffered saline at 25° C and kept them under vigorous stirring (700 RPM) using an Eppendorf Thermomixer (PN: 5382000023)[26] to promote passive monolayer desorption.

Interrogation of the sensors via cyclic voltammetry at a slow voltage scanning rate (0.1 V/s) revealed a 50% increase in oxygen reduction current at −0.5 V vs Ag|AgCl after 14 days, when the DNA packing density was below 1 pmol/cm^2 (Figure 2A, B). In contrast, we observed a smaller 35% increase in oxygen reduction currents for NBEs prepared using the higher packing density of ∼4 pmol/cm^2 (Figure 2C). However, we observed no significant change in the capacitive currents of the voltammograms at, for example, −0.1 V, regardless of the DNA packing density. This last observation is an indication that blocking monolayer elements mostly remain on the sensor surface after 14 days. The increase in oxygen reduction currents could be due to monolayer reorganization, which can drive the formation of defects or pinholes.[27,28] Interrogating the sensors at a 10-fold faster voltage scanning rate (1 V/s) showed less than 15% change in oxygen reduction currents, regardless of the DNA packing density (Figure S1), and again no change in capacitive currents, confirming that blocking monolayer elements are almost fully retained after 14 days even under vigorous stirring at 25° C. Comparing the capacitive currents at t = 0 and t = 14 days relative to those measured on a bare gold electrode (Figure 2D), we confirmed that blocking monolayer elements remain on the electrode surface and that the observed increases in oxygen reduction currents are negligible relative to the faradaic currents observed on unfunctionalized electrodes. Finally, interrogating the sensors via square wave voltammetry resulted in voltammograms with identical peak currents when the sensors were functionalized with DNA packing density <1 pmol/cm^2 (Figure S2A). Sensors functionalized with a DNA packing density higher than 1 pmol/cm^2 showed ∼20% decay in voltammogram peak currents (Figure S2B,C). Although measurable, such a current decay occurred over a span of 2 weeks and is too small to account for the significant signal decay observed when NBEs are serially interrogated by voltammetry in buffered saline.

NBEs' Signal Stability Strongly Depends on Voltage Window. The majority of NBEs reported in the literature for continuous molecular monitoring rely on the use of methylene blue as their redox reporter. Although this molecule has so far shown superior sensing performance relative to other reporters,[29] its formal reduction potential ($E^{0\prime}$ = −0.24 V vs Ag|AgCl) requires the use of a voltage window that promotes NBE monolayer desorption (Figure 1C). In a previous report, Leung et al. showed that centering the voltage window closely around methylene blue's voltammetric peak could decrease voltage-induced NBE damage.[18] Watkins et al. have also demonstrated that although repetitive voltage scanning can damage monolayers in buffered saline, frequent modulation of the electrode field may help electrostatically prevent fouling in

https://doi.org/10.1021/acs.analchem.2c05158
Anal. Chem. 2023, 95, 4974−4983

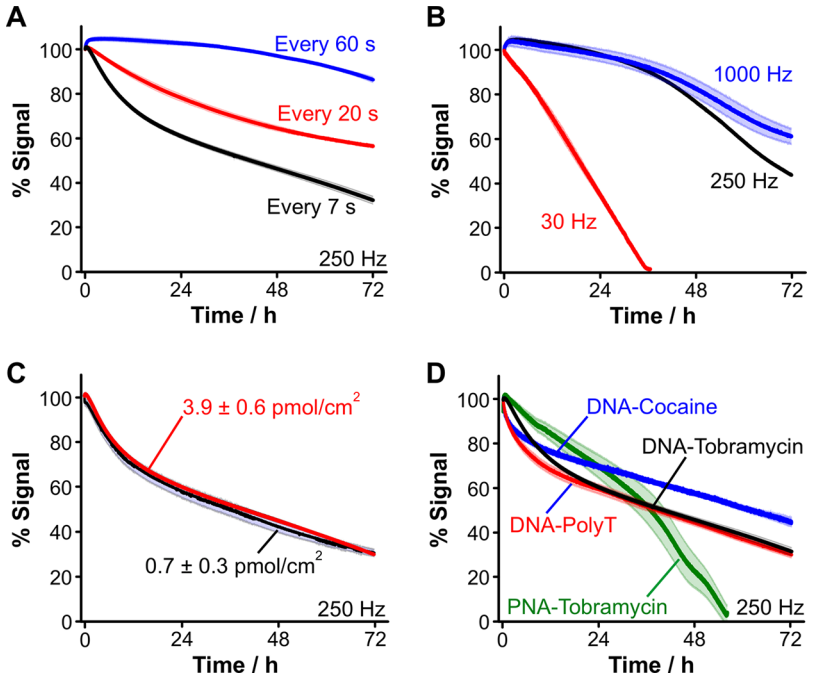

Figure 4. Effect of voltammetric parameters and monolayer composition on NBE stability. (A) NBE interrogation frequency has a strong effect on signal stability. Here, we show voltammetric peak currents measured at 250 Hz via square wave voltammetry at three different measurement frequencies. (B) Square wave frequency, a technique parameter, also affects NBE signal lifetimes. The signal of NBEs that were interrogated at 1000 Hz decayed at a rate seven-times slower than sensors interrogated at 30 Hz. The total number of interrogations (8,600) is the same across all frequencies. (C) No correlation was observed between DNA packing density (Γ_{100nM} = 0.7 ± 0.3 pmol/cm^2, Γ_{2000nM} = 3.9 ± 0.6 pmol/cm^2) and the signal decay rate. The subscript indicates the molar concentration of DNA used in the deposition vat. (D) NBE decay rates are similar across three different DNA sequences, including a triple foil structure (cocaine aptamer), a hairpin (tobramycin aptamer), and a linear strand (poly-dT). However, changing the phosphate backbone for the peptidic chain in PNA resulted in faster signal decay. All traces show the average of n = 6 individual sensors, and shaded areas are their standard deviation.

biofluids.[30] Here, we expand on this prior knowledge to demonstrate that interrogation of methylene blue per se causes significant sensor damage in phosphate-buffered saline, and that new redox reporters with more positive reduction potentials are critically needed to improve sensor stability under continuous voltammetric interrogation. With the availability of new reporters with positive redox potentials, field modulation at the sensor surface to prevent fouling may still be needed.

To illustrate the negative effect that methylene blue interrogation has on NBE stability, we interrogated two batches of NBEs every 7 s for 24 h via square wave voltammetry at 250 Hz across two independent voltage windows: Batch 1 was interrogated across the methylene blue voltage window ranging from −0.1 to −0.5 V, and Batch 2 was interrogated between −0.2 and 0.2 V. Comparing Batch 1 voltammograms (red traces) measured at t = 0 h (Figure 3A) vs t = 24 h (after 12,000 scans, Figure 3B), we observed a 40% decrease in voltammetric peak currents from the reduction of methylene blue (Figure 3C). Such a current decrease was not accompanied by changes in NBE capacitive currents (black trace in Figure 3C), an indication that only methylene blue-functionalized DNA elements were lost, but the blocking MCH monolayer remained. Similarly, Batch 2 voltammograms (blue traces in Figure 3A,B) showed no changes in capacitive currents (Figure 3D). However, in contrast to Batch 1, interrogation of Batch 2 across methylene blue's voltage window once at t = 0 h (top dashed panel) and once at t = 24 h (i.e., after ∼12,000 scans, bottom dashed panel) showed 99% retention of methylene blue reduction currents. These results indicate that the interrogation of NBEs in the voltage window between −0.2 and 0.2 V vs Ag|AgCl does not affect sensor stability. This is not surprising, as voltages more positive than 0.2 V can generate incipient surface oxides on gold electrodes,[31] damaging the NBE monolayer, and voltages more negative than −0.2 V can drive the reduction of molecular oxygen on gold through monolayer defects, generating peroxide radicals[32] that are known to damage NBE monolayers.[33] A recent report from our laboratory demonstrates that the osmium-based redox reporter, [Os-(dmebpy)$_2$Cl(ampy)]$^+$, which has a formal reduction potential of ∼0.18 V vs Ag|AgCl, achieves 35% better operational stability relative to methylene blue under continuous voltammetric cycling.[34] Additionally, Li et al. have published a novel redox reporter based on tetrathiafulvalene,[35] which undergoes reversible and pH-insensitive electron transfer when bound to DNA and has a reduction potential of $E^{0\prime}$ ∼ 0.05 V vs Ag|AgCl, right at the center of the stability window of NBEs. Although no conclusive stability data is provided in their initial report, the reduction potential of this reporter may dramatically improve NBE lifetimes.

NBE Stability Is a Strong Function of Interrogation and Square Wave Frequency. We next studied the effect of varying electrochemical interrogation parameters on NBE stability. In a previous study,[8] we reported that serially interrogating NBEs via square wave voltammetry every 12 h achieved stable sensing with less than 5% signal decay over a 72 h period. However, such a slow interrogation frequency may be impractical from the perspective of continuous molecular monitoring applications, so here, we set out to

https://doi.org/10.1021/acs.analchem.2c05158
Anal. Chem. 2023, 95, 4974−4983

further understand the effect of interrogation frequency on NBE stability. For this study, we investigated three different interrogation frequencies: one measurement every 7, 20, or 60 s. In these measurements, we kept all square wave voltammetry parameters constant (using a square wave frequency of 250 Hz and an amplitude of 50 mV) and only adjusted the pause interval between voltammetric scans. Doing so, we observed that NBE stability is a strong function of sensor interrogation frequency (Figure 4A). Specifically, sensors interrogated every 60 s resulted in voltammetric peak current vs time plots showing 50% more current after 72 h (~4200 scans) relative to sensors interrogated every 7 s (~37,000 scans over the same period). At an intermediate interrogation frequency of one measurement every 20 s (~12,500 scans), we observed intermediate NBE stability. Given that negative voltage scanning damages NBEs (Figures 1C and 3C), these last results indicate that more frequent sensor biasing at voltages more negative than −0.2 V causes faster NBE signal decay.

NBE signal decay is also a function of the electrochemical parameters used during interrogation. Specifically, the frequency of the square waveform used during voltammetric interrogation can significantly affect NBE stability by dictating how long the voltage is biased at a given value per square pulse, with faster frequencies minimizing the time continuously spent at voltages more negative than −0.2 V. To illustrate this effect, we independently interrogated three batches of sensors using a square wave frequency of either 30, 250, or 1000 Hz. To deconvolute the effect of measurement frequency from the effect of square wave frequency, we set a pause interval between measurements so that the same number of voltammetric scans (8600 scans) were performed over the measurement period regardless of square wave frequency. Sensors interrogated at 1000 Hz displayed the longest stability (blue trace in Figure 4B). In contrast, sensors interrogated at 30 Hz decayed at a sixfold faster rate, with complete loss of methylene blue reduction peaks at ~30 h. We speculate that at low frequencies, the longer duration of each square wave pulse drives oxygen reduction under diffusion control at monolayer defects, generating peroxide species that can react with monolayer elements, removing them from the surface.[32,36,37] At higher frequencies, oxygen reduction is not under diffusion control and occurs to a lower extent, causing less damage.

Number of Nucleic Acids on the Electrode Surface Does Not Play a Role in Signal Loss. After the experiments shown in Figure 3, which indicate that nucleic acid loss rather than full monolayer desorption is the driving force of signal decay, we evaluated the role that nucleic acid density on electrode surfaces plays on NBE stability. To evaluate this role, we independently functionalized two electrode batches with different packing densities of a tobramycin-binding aptamer[21] spanning the range commonly used for NBE sensing: Γ_{100nM} = 0.7 ± 0.3 pmol/cm^2 and Γ_{2000nM} = 3.9 ± 0.6 pmol/cm^2. When we serially interrogated the sensors every 7 s for 72 h at a square wave frequency of 250 Hz, we observed that the NBE signal decay across both batches was within measurement error (Figure 4C). These results indicate that, although DNA packing density plays a key role in the analytical performance of NBEs,[38,39] it does not seem to affect their operational stability.

Nucleic Acid Chemistry Can Directly Affect NBEs' Signal Stability. To investigate this effect, we independently functionalized batches of sensors with either a 30-nucleotide-long, cocaine-binding aptamer that folds into a three-way junction,[40] a 26-nucleotide-long tobramycin-binding aptamer that folds into a hairpin structure,[41] a 26-nucleotide-long poly-dT linear strand, and the same tobramycin-binding aptamer but made of peptide nucleic acids (PNA).[42] Interrogating the resulting sensors via square wave voltammetry every 7 s for 72 h, we observed that NBE signals decayed at similar rates for the three DNA sequences based on naturally occurring nucleic acids, albeit with small differences in the first hours likely due to structural differences between the sequences. In contrast, the PNA-functionalized sensors decayed at a faster rate, with complete disappearance of methylene blue currents at ~50 h. We speculate this is caused by the action of reactive peroxide species formed during the reduction of molecular oxygen at monolayer defects, which are expected to react more readily with the amide bonds[43] in PNA than with the phosphate bonds in DNA.[44] This idea is supported by square wave voltammograms measured at t = 0 and t = 48 h on the same PNA-based NBEs (Figure S3), which show significant increases in capacitive and oxygen reduction currents relative to DNA-based analogues. A recent publication by Barroso-Martínez et al. reports a novel redox reporter that can chemically trap reactive oxygen species and allow their electrochemical quantification on electrode surfaces.[45] Such measurements are beyond the scope of this work but could be used to further understand the rates of NBE signal decay as a function of nucleic acid chemistries.

To discard the possibility that NBE signal decay is due to the loss of methylene blue reporters and not to the loss of nucleic acids, we employed the method developed by Steel, Herne, and Tarlov to quantitatively measure surface DNA concentrations.[23,46] This method is based on exposing gold surfaces functionalized with nucleic acids to a solution of ruthenium hexamine at low ionic strength. The ruthenium complex is positively charged (3+) and strongly binds to the negatively charged backbone of the nucleic acids (not in the case of PNA). Chronocoulometric interrogation of the nucleic acid-bound ruthenium hexamine complexes (see Methods in Supporting Information) in buffered solutions allows stoichiometric quantification of nucleic acids. Using this method on NBEs identical to the ones shown in Figure 4C, at t = 0 h and at t = 72 h after having serially interrogated the NBEs every 7 s (i.e., ~37,000 scans), we measured a 70% loss in surface nucleic acid concentration (Figure S4) that matched the decay of methylene blue's currents observed in Figure 4C. These results confirmed that NBE signal loss is due to desorption of nucleic acids, with concomitant loss of their covalently bound reporters from the electrode surface.

Mechanisms of Signal Loss in Biological Media. Our results so far demonstrate that voltage-induced monolayer desorption (Figure 1C) is the main driving factor of methylene blue-dependent NBE signal decay in buffered solutions. However, when NBEs are deployed in biological fluids, additional factors can accelerate sensor signal decay. In this section, we demonstrate, for the first time, that competitive displacement of monolayer elements by naturally occurring thiols (Figure 1D) is one of the main drivers of NBE sensor decay in biofluids. Additionally, we show that non-specific protein binding does not accelerate the decay but, instead, seems to protect sensor surfaces by coating them, thereby slowing down the loss of NBE monolayer elements.

To independently study the effect that competitive displacement (Figure 1D) and non-specific protein binding (Figure 1E) have on NBE stability, we developed serum mimetics

https://doi.org/10.1021/acs.analchem.2c05158
Anal. Chem. 2023, 95, 4974−4983

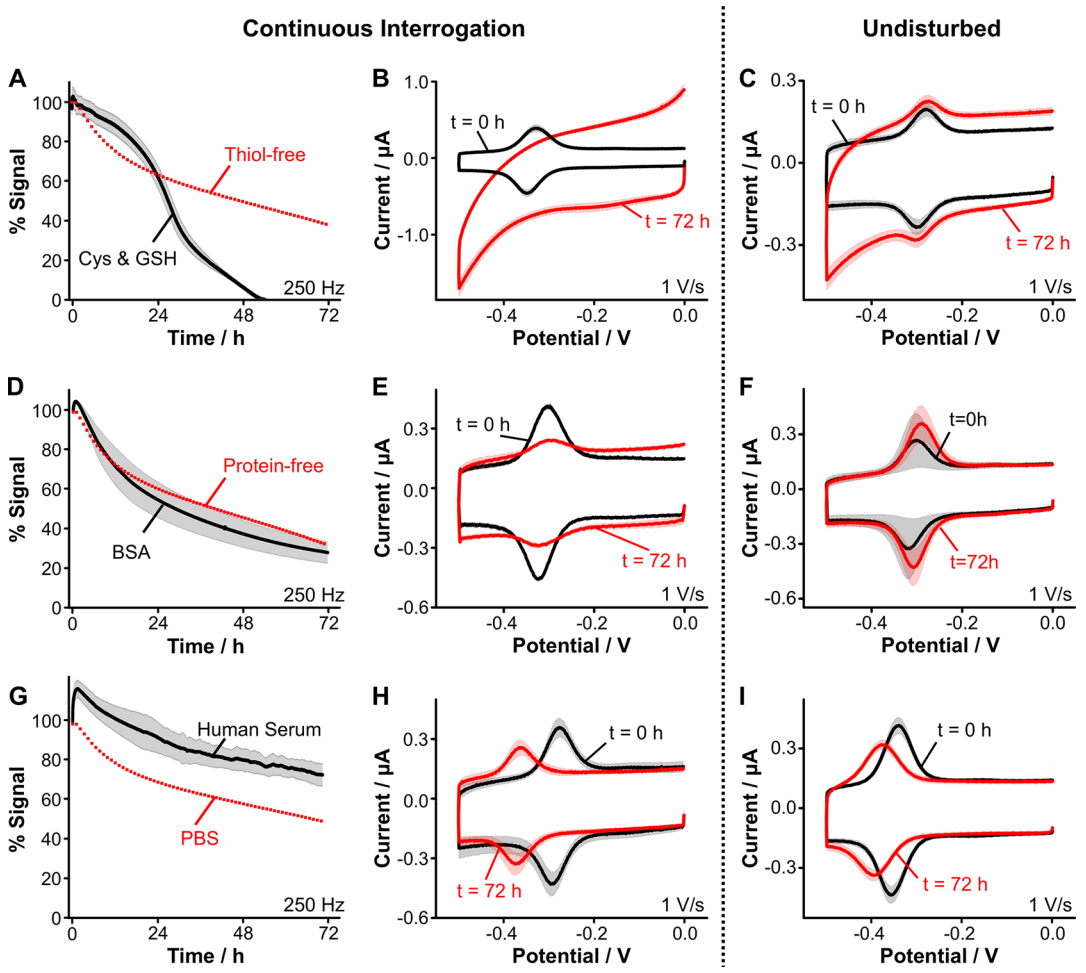

Figure 5. Degradation pathways of NBEs in biological media. (A) NBEs interrogated by square wave voltammetry in the presence of reduced glutathione (5 μM) and oxidized cysteine (250 μM) at their physiological concentrations showed complete disappearance of MB redox peaks at 48 h. Red dashed lines correspond to the mean from Figure 4C. (B) Cyclic voltammograms measured at t = 0 h and t = 72 h after serial interrogation revealed a considerable increase in capacitive and oxygen reduction currents. (C) In contrast, sensors immersed in the same solution for the same period but without serial interrogation showed less current changes at 72 h. (D) NBEs serially interrogated by square wave voltammetry in the presence of physiological concentrations of serum albumin (700 μM) presented a signal decay similar in magnitude and shape to the decay observed in protein-free solutions (red trace). (E) Cyclic voltammograms showed a proportional decrease in MB redox peaks and an increase in capacitive and oxygen reduction currents. (F) However, NBEs that were incubated in albumin solutions but were interrogated only twice showed a 30% increase in methylene blue redox peaks without changes to capacitive currents. (G) NBEs serially interrogated in undiluted human serum showed decay traces with a similar rate relative to those observed in buffered saline. (H) Cyclic voltammograms showed a decrease in MB redox peaks caused by serial interrogation, without appreciable changes to capacitive or oxygen reduction currents. (I) NBEs immersed in serum but only interrogated twice over the 72 h-period displayed a less pronounced decay in MB redox peaks relative to NBEs that were serially interrogated. Continuous interrogation of NBEs was carried out in all cases using a square wave frequency of 250 Hz and an amplitude of 50 mV, interrogating the sensors every 7 s. The CV scan rate was 1 V/s. Solid lines and shaded areas represent the average and standard deviation of n = 8 electrodes.

containing specific molecular compositions based on the most abundant thiolated molecules found in serum. We used serum as a model system because this biological fluid is frequently used for bioassays in the clinic,[47] and it is the fluid where NBE-based continuous molecular measurements have been most frequently performed.[9,14,48] The two most abundant thiolated small molecules found in serum are cysteine and glutathione.[49,50] Cysteine is naturally >98% oxidized and present at an average concentration of 250 μM in healthy adults, while glutathione is 2% in its oxidized form and typically found at a concentration of 5 μM (Table S1).[49,50] Protein wise, the most abundant molecule is albumin,[51] found at an average concentration of 700 μM and accounting for 60% of all proteins found in serum.[51] To create our mimetics, we prepared three phosphate-buffered saline solutions containing either two thiolated small molecules, serum albumin, or a mixture of all three molecules, always at their physiological concentrations.

Competitive displacement by thiolated small molecules strongly drives NBE signal decay, with the rate of the decay being accelerated by frequent sensor interrogation. To demonstrate this, we immersed NBEs in our serum mimetic containing oxidized cysteine and reduced glutathione and serially interrogated them every 7 s for 72 h using a square wave frequency of 250 Hz. Doing so, we observed that NBE signal decay was approximately twofold faster in our mimetic (Figure 5A) than the decay observed in the absence of the small thiolated molecules (Figure 4C). Using cyclic voltammetry to further characterize the NBE surfaces, at 72 h, we observed complete disappearance of methylene blue's redox

https://doi.org/10.1021/acs.analchem.2c05158
Anal. Chem. 2023, 95, 4974−4983

peaks (Figure 5B), a tripling of capacitive currents relative to the initial voltammogram measured at t = 0 h, and a considerable increase of oxygen reduction currents. Comparing such cyclic voltammograms against those measured on equivalent NBEs exposed to the same serum mimetic but only interrogated twice, once at t = 0 h and once at t = 72 h (Figure 5C), we observed considerably less NBE monolayer decay when the sensors were not continuously interrogated (red traces, Figure 5C vs 5B). Overall, these results indicate that NBE decay in biological fluids is more pronounced when both competitive displacement (Figure 1D) and voltage-induced desorption of monolayer elements (Figure 1C) occur simultaneously.

In contrast to the results observed in the presence of small thiolated molecules, NBEs that were exposed to the serum mimetic containing albumin showed the same decay under continuous interrogation (∼65% at 72 h, Figure 5D) relative to sensors exposed to buffered saline (red dashed line in Figure 5D). Further evaluation of these sensors by cyclic voltammetry at t = 0 h and after t = 72 h of continuous interrogation resulted in voltammograms that showed a proportional decrease of methylene blue peaks (i.e., 65%) and a small but statistically significant change in capacitive currents (Figure 5E). We postulate that these results reflect two competing processes: on the one hand, non-specific protein binding forms a coating on the sensor that pushes methylene blue closer to the surface, increasing faradaic currents (seen as a rise in currents at t < 1 h in Figure 5D, G). On the other hand, frequent voltammetric interrogation causes voltage-induced desorption of sensor monolayer elements, decreasing faradaic currents and inducing monolayer reorganization that results in increased capacitive currents. To evaluate this hypothesis, we compared the voltammograms shown in Figure 5E against voltammograms measured on NBEs that were only interrogated once at t = 0 h and once at t = 72 h (Figure 5F). In the absence of frequent sensor interrogation, we confirmed that the capacitive currents of NBEs did not change and the faradaic peaks from methylene blue increased in magnitude over time, reflecting a pushing effect that protein binding has on the relative proximity of methylene blue probes to the sensor surface (also shown by square wave voltammograms in Figure S5).

The serum mimetics used in this work allowed us to independently study the effects of competitive displacement and non-specific protein binding on NBEs' sensor stability. However, such buffered solutions do not fully reflect the molecular complexity of undiluted human serum. We illustrate this point here by performing the same voltammetric analysis on a new batch of NBEs immersed in undiluted human serum. The peak current vs time trace (Figure 5G) showed a short-lived rise (due to non-specific protein binding) and long decay that were similar in trend to those observed when using the protein mimetic (see Figure 5D); however, the magnitude of the decay was 30% smaller. We speculate this is because serum contains 40% of other polyelectrolytes in addition to serum albumin,[51] which may contribute to a faster formation of the protein corona on the sensor surface, slowing down monolayer desorption. The shift in peak position observed in Figure 5H likely reflects the junction potential caused by a difference in viscosity between the reference electrode solution (Ag|AgCl with KCl in water) and human serum. When we repeated the measurements on NBEs that were only interrogated twice, we observed a measurable decrease in the magnitude of methylene blue's redox peaks after 72 h (Figure 5I). This signal decay was smaller in magnitude relative to the decrease observed in continuously interrogated sensors (Figure 5H), but obviously different to the increase observed with the albumin mimetic (Figure 5F). We note that, unlike our albumin mimetic, undiluted human serum contains glutathione and cysteine. It also contains other proteins that contribute to surface fouling, protecting the sensor surface. Thus, differences in voltammograms between Figure 5F,I can be attributed to differences in the composition of the medium, with the real serum being richer in molecular diversity and, therefore, driving competing effects on NBE surfaces.

As a last control to confirm the effect of prolonged serum exposure on the sensors, we performed cyclic voltammetry measurements in NBEs that were incubated in undiluted serum for two periods, 2 h vs 72 h, and then washed with 8 M urea to remove any surface-bound proteins (Figure S6). First, we tested the effect of exposing the sensors to the 8 M urea bath for 20 min under continuous shaking (in a thermomixer at 400 rpm) and observed no damage to the NBE monolayer (Figure S6A). Next, we interrogated a new batch of NBEs in buffered saline, then exposed the sensors to serum for 2 h, washed them with urea for 20 min under shaking, and interrogated the sensors again in buffered saline (Figure S6B). The results of this experiment show that an 8 M urea wash is effective at fully removing non-specifically bound protein from the NBE surface, regenerating the magnitude of the NBE voltammograms. However, if the experiment is repeated but the NBEs are incubated in serum for 72 h, the urea wash does not regenerate the signal (Figure S6C). As discussed in the previous paragraph, we believe this is due to the competitive displacement of the NBE monolayer by naturally occurring thiols, a process that occurs more visibly over 72 h of continuous exposure to serum. In contrast, non-specific protein binding occurs within the first 2 h and can be corrected ex situ via urea washing (Figure S6B). However, the formation of the protein biofilm, if effective at protecting against naturally occurring nucleases,[13] may be less effective at filtering out thiolated small molecules that can still displace NBE monolayer elements and cause signal loss.

CONCLUSIONS

We report a systematic study of four main mechanisms of nucleic acid-based electrochemical sensor (NBE) signal decay under continuous voltammetric interrogation in phosphate-buffered saline and in undiluted human serum. Our results indicate that the signal of NBEs placed in undiluted serum decays via two main mechanisms: voltage-induced monolayer desorption (Figure 1C) and competitive displacement (Figure 1D). An additional contributing factor to signal decay is the presence of nucleases in the serum, which can hydrolyze nucleic acids, thereby contributing to sensor decay. This last effect, however, occurs at significantly slower rates than voltage-induced desorption and competitive displacement of NBE monolayers.[14] Evaluating the effect of voltage magnitude on NBE signal decay, we determined that using a sensor interrogation window between −0.2 and 0.2 V vs Ag|AgCl achieves the best stability, eliminating voltage-induced sensor damage. These results highlight the need for novel redox reporters that undergo electron transfer at redox potentials contained within that voltage window. To overcome competitive displacement, we postulate that future NBE development must incorporate polyvalent monolayer chem-

https://doi.org/10.1021/acs.analchem.2c05158
Anal. Chem. 2023, 95, 4974−4983

istries and/or monolayers with steric properties that can resist direct displacement by naturally occurring monovalent thiols. In summary, this work provides a mechanistic framework to understand NBE signal decay under continuous voltammetric interrogation and suggests steps to improve sensor stability toward realizing stable, multiday NBE-based molecular monitoring in the body.

■ ASSOCIATED CONTENT

Supporting Information

The Supporting Information is available free of charge at https://pubs.acs.org/doi/10.1021/acs.analchem.2c05158.

Expanded methods including reagents, materials, and protocols and figures depicting sensor stability (PDF)

■ AUTHOR INFORMATION

Corresponding Author

Netzahualcóyotl Arroyo-Currás − *Chemistry-Biology Interface Program, Zanvyl Krieger School of Arts & Sciences, Johns Hopkins University, Baltimore, Maryland 21218, United States; Department of Pharmacology and Molecular Sciences, Johns Hopkins University School of Medicine, Baltimore, Maryland 21205, United States;* orcid.org/0000-0002-2740-6276; Phone: 443-287-4798; Email: netzarroyo@jhmi.edu

Authors

Vincent Clark − *Chemistry-Biology Interface Program, Zanvyl Krieger School of Arts & Sciences, Johns Hopkins University, Baltimore, Maryland 21218, United States;* orcid.org/0000-0001-9707-8004

Miguel Aller Pellitero − *Departamento de Química Física y Analítica, Universidad de Oviedo, Oviedo 33006, Spain; Instituto de Investigación Sanitaria Del Principado de Asturias, Oviedo 33011, Spain; Department of Pharmacology and Molecular Sciences, Johns Hopkins University School of Medicine, Baltimore, Maryland 21205, United States*

Complete contact information is available at: https://pubs.acs.org/10.1021/acs.analchem.2c05158

Author Contributions

#V.C. and M.A.P. contributed equally. V.C., M.A.P., and N.A.C. developed the concept; and V.C., and M.A.P. performed all the experiments. All authors participated in the writing and editing of the manuscript.

Notes

The authors declare no competing financial interest.

■ ACKNOWLEDGMENTS

This work was supported by the National Institute of General Medical Sciences of the National Institutes of Health under Award Number R01GM140143. The content is solely the responsibility of the authors and does not necessarily represent the official views of the National Institutes of Health. V.C. thanks the NSF for providing support in the form of a Graduate Research Fellowship (#2139757) to support his graduate education and training. M.A.P. thanks Fundación Científica Asociación Española Contra el Cáncer (AECC) for the postdoctoral fellowship supporting his work.

■ REFERENCES

(1) Wu, Y.; Arroyo-Currás, N. *Curr. Opin. Electrochem.* **2021**, *27*, 100695.
(2) Shaver, A.; Arroyo-Currás, N. *Curr. Opin. Electrochem.* **2022**, *32*, 100902.
(3) Pellitero, M. A.; Shaver, A.; Arroyo-Currás, N. *J. Electrochem. Soc.* **2019**, *167*, 037529.
(4) Arroyo-Currás, N.; Dauphin-Ducharme, P.; Scida, K.; Chávez, J. L. *Anal. Methods* **2020**, *12*, 1288−1310.
(5) Arroyo-Currás, N.; Somerson, J.; Vieira, P. A.; Ploense, K. L.; Kippin, T. E.; Plaxco, K. W. *PNAS* **2017**, *114*, 645−650.
(6) Das, J.; Gomis, S.; Chen, J. B.; Yousefi, H.; Ahmed, S.; Mahmud, A.; Zhou, W.; Sargent, E. H.; Kelley, S. O. *Nat. Chem.* **2021**, *13*, 428−434.
(7) Baker, B. R.; Lai, R. Y.; Wood, M. S.; Doctor, E. H.; Heeger, A. J.; Plaxco, K. W. *J. Am. Chem. Soc.* **2006**, *128*, 3138−3139.
(8) Lubin, A. A.; Plaxco, K. W. *Acc. Chem. Res.* **2010**, *43*, 496−505.
(9) Swensen, J. S.; Xiao, Y.; Ferguson, B. S.; Lubin, A. A.; Lai, R. Y.; Heeger, A. J.; Plaxco, K. W.; Soh, H. T. *J. Am. Chem. Soc.* **2009**, *131*, 4262−4266.
(10) Dauphin-Ducharme, P.; Arroyo-Currás, N.; Kurnik, M.; Ortega, G.; Li, H.; Plaxco, K. W. *Langmuir* **2017**, *33*, 4407−4413.
(11) Mahlum, J. D.; Pellitero, M. A.; Arroyo-Currás, N. *J. Phys. Chem. C* **2021**, *125*, 9038−9049.
(12) Arroyo-Currás, N.; Dauphin-Ducharme, P.; Ortega, G.; Ploense, K. L.; Kippin, T. E.; Plaxco, K. W. *ACS Sens* **2018**, *3*, 360−366.
(13) Shaver, A.; Kundu, N.; Young, B. E.; Vieira, P. A.; Sczepanski, J. T.; Arroyo-Currás, N. *Langmuir* **2021**, *37*, 5213−5221.
(14) Shaver, A.; Curtis, S. D.; Arroyo-Currás, N. *ACS Appl. Mater. Interfaces* **2020**, *12*, 11214−11223.
(15) Wu, Y.; Tehrani, F.; Teymourian, H.; Mack, J.; Shaver, A.; Reynoso, M.; Kavner, J.; Huang, N.; Furmidge, A.; Duvvuri, A.; Nie, Y.; Laffel, L. M.; Doyle, F. J.; Patti, M.-E.; Dassau, E.; Wang, J.; Arroyo-Currás, N. *Anal. Chem.* **2022**, *94*, 8335−8345.
(16) Lin, S.; Cheng, X.; Zhu, J.; Wang, B.; Jelinek, D.; Zhao, Y.; Wu, T.-Y.; Horrillo, A.; Tan, J.; Yeung, J.; Yan, W.; Forman, S.; Coller, H. A.; Milla, C.; Emaminejad, S. *Sci. Adv.* **2022**, *8*, No. eabq4539.
(17) Pellitero, M. A.; Curtis, S. D.; Arroyo-Currás, N. *ACS Sens* **2021**, *6*, 1199−1207.
(18) Leung, K. K.; Downs, A. M.; Ortega, G.; Kurnik, M.; Plaxco, K. W. *ACS Sens* **2021**, *6*, 3340−3347.
(19) Li, H.; Dauphin-Ducharme, P.; Arroyo-Currás, N.; Tran, C. H.; Vieira, P. A.; Li, S.; Shin, C.; Somerson, J.; Kippin, T. E.; Plaxco, K. W. *Angew. Chem. Int. Edit.* **2017**, *56*, 7492−7495.
(20) Arroyo-Currás, N.; Scida, K.; Ploense, K. L.; Kippin, T. E.; Plaxco, K. W. *Anal. Chem.* **2017**, *89*, 12185−12191.
(21) Schoukroun-Barnes, L. R.; Wagan, S.; White, R. J. *Anal. Chem.* **2014**, *86*, 1131−1137.
(22) Curtis, S. D.; Ploense, K. L.; Kurnik, M.; Ortega, G.; Parolo, C.; Kippin, T. E.; Plaxco, K. W.; Arroyo-Currás, N. *Anal. Chem.* **2019**, *91*, 12321−12328.
(23) Clark, V.; Waters, K.; Orsburn, B.; Bumpus, N. N.; Kundu, N.; Sczepanski, J. T.; Ray, P.; Arroyo-Currás, N. *Angew. Chem. Int. Edit. n* **2022**, *61*, No. e202211292.
(24) Pellitero, M. A.; Arroyo-Currás, N. *Anal. Bioanal. Chem.* **2022**, *414*, 5627−5641.
(25) Schlenoff, J. B.; Li, M.; Ly, H. *J. Am. Chem. Soc.* **1995**, *117*, 12528−12536.
(26) EppendorfC - Instruments, T.hermoMixer® Temperature Control and Mixing - Eppendorf US. accessed 20 10, 2022, 2022.https://online-shop.eppendorf.us/US-en/Temperature-Control-and-Mixing-44518/Instruments-44519/Eppendorf-ThermoMixerC-PF-19703.html.
(27) Polohová, V.; Šnejdárková, M.; Podskočová, J.; Svobodová, L.; Chorvát, D., Jr.; Hianik, T. *Electroanalysis* **2007**, *19*, 324−330.
(28) Mougari, A.; Zabat, M.; Boudjadar, S. *Surf. Rev. Lett.* **2019**, *26*, 1950067.

(29) Kang, D.; Ricci, F.; White, R. J.; Plaxco, K. W. *Anal. Chem.* **2016**, *88*, 10452−10458.
(30) Watkins, Z.; Karajić, A.; Young, T.; White, R.; Heikenfeld, J. *Chemistry* **2022**, DOI: 10.26434/chemrxiv-2022-s1qj9.
(31) Rodríguez-López, J.; Alpuche-Avilés, M. A.; Bard, A. J. *J. Am. Chem. Soc.* **2008**, *130*, 16985−16995.
(32) Yu, H.-Y.; Li, X.-F.; Zhang, T.-H.; Liu, J.; Tian, J.-H.; Yang, R. *ChemSusChem* **2020**, *13*, 2702−2708.
(33) Chung, J.; Sepunaru, L.; Plaxco, K. W. *ECS Sens. Plus* **2022**, *1*, 011604.
(34) Aller Pellitero, M. A.; Kundu, N.; Sczepanski, J.; Arroyo-Currás, N. *Analyst* **2023**, *148*, 806.
(35) Li, S.; Ferrer-Ruiz, A.; Dai, J.; Ramos-Soriano, J.; Du, X.; Zhu, M.; Zhang, W.; Wang, Y.; Herranz, M.; Jing, L.; Zhang, Z.; Li, H.; Xia, F.; Martín, N. *Chem. Sci. J.* **2022**, *13*, 8813−8820.
(36) Wang, K.; Huang, J.; Chen, H.; Wang, Y.; Song, S. *Chem. Commun.* **2020**, *56*, 12109−12121.
(37) Zhao, X.; Liu, Y. *J. Am. Chem. Soc.* **2021**, *143*, 9423−9428.
(38) White, R. J.; Phares, N.; Lubin, A. A.; Xiao, Y.; Plaxco, K. W. *Langmuir* **2008**, *24*, 10513−10518.
(39) Liu, Y.; Canoura, J.; Alkhamis, O.; Xiao, Y. *ACS Appl. Mater. Interfaces* **2021**, *13*, 9491−9499.
(40) Cekan, P.; Jonsson, E. Ö.; Sigurdsson, S. *Nucleic Acids Res.* **2009**, *37*, 3990−3995.
(41) Jiang, L.; Patel, D. J. *Nat. Struct. Mol. Biol.* **1998**, *5*, 769−774.
(42) Egholm, M.; Buchardt, O.; Nielsen, P. E.; Berg, R. H. *J. Am. Chem. Soc.* **1992**, *114*, 1895−1897.
(43) Hawkins, C. L.; Davies, M. J. *JBC* **2019**, *294*, 19683−19708.
(44) Cooke, M. S.; Evans, M. D.; Dizdaroglu, M.; Lunec, J. *FASEB J.* **2003**, *17*, 1195−1214.
(45) Barroso-Martínez, J. S.; Romo, B.; Putnam, S.; Bustos, S. T.; Rodríguez-López, E.; Rodríguez-López, J. *J. Am. Chem. Soc.* **2022**, *144*, 18896−18907.
(46) Steel, A. B.; Herne, T. M.; Tarlov, M. J. *Anal. Chem.* **1998**, *70*, 4670−4677.
(47) Fanali, G.; di Masi, A.; Trezza, V.; Marino, M.; Fasano, M.; Ascenzi, P. *Mol. Aspects Med.* **2012**, *33*, 209−290.
(48) Xiao, Y.; Lubin, A. A.; Heeger, A. J.; Plaxco, K. W. *Angew. Chem. Int. Edit.* **2005**, *117*, 5592−5595.
(49) Oliveira, P. V. S.; Laurindo, F. R. M. *Clin. Sci.* **2018**, *132*, 1257−1280.
(50) Fu, X.; Cate, S. A.; Dominguez, M.; Osborn, W.; Özpolat, T.; Konkle, B. A.; Chen, J.; López, J. A. *Sci. Rep.* **2019**, *9*, 115.
(51) 5 Human Albumin. *Transfus Med Hemother* **2009**, *36* (), 399−407.

https://doi.org/10.1021/acs.analchem.2c05158
Anal. Chem. 2023, 95, 4974−4983